Geochemical Journal, Vol. 47, pp. 119 to 135, 2013

^{230}Th-normalized fluxes of biogenic components from the central and southernmost Chilean margin over the past 22,000 years

MIHO FUKUDA,[1,2]* NAOMI HARADA,[2] MIYAKO SATO,[2] CARINA B. LANGE,[3] NAOKAZU AHAGON,[4] HAJIME KAWAKAMI,[5] WATARU MIYASHITA,[6] SILVIO PANTOJA,[3] TAKESHI MATSUMOTO[7] and ISAO MOTOYAMA[8]

[1]Department of Earth and Evolution Sciences, University of Tsukuba, 1-1-1 Tenno-dai, Tsukuba 305-8572, Japan
[2]Research Institute for Global Change, Japan Agency for Marine-Earth Science and Technology, 2-15 Natsushima-cho, Yokosuka 237-0061, Japan
[3]COPAS Center and Department of Oceanography, University of Concepción, P.O. Box 160-C, Concepción, Chile
[4]Kochi Core Center, Japan Agency for Marine-Earth Science and Technology, 200 Minobe Otsu, Nankoku, Kochi 783-8502, Japan
[5]Mutsu Institute for Oceanography, Japan Agency for Marine-Earth Science and Technology, 690 Kitasekine, Sekine, Mutsu 035-0022, Japan
[6]Fast Breeder Reactor (FBR) Technology Engineering Services Company, 2-2-2 Chuo-cho, Suruga 914-0811, Japan
[7]Physics and Earth Sciences, Graduate School of Engineering and Science, University of the Ryukyu, 1 Senbaru, Nishihara-cho, Okinawa 903-0129, Japan
[8]Department of Earth and Environmental Sciences, Faculty of Science, Yamagata University, 1-4-12, Kojirakawa-machi, Yamagata 990-8560, Japan

(*Received April 4, 2012; Accepted September 19, 2012*)

We report on ^{230}Th-normalized fluxes of biogenic components—total organic carbon (TOC), total nitrogen (TN), calcium carbonate ($CaCO_3$), and biogenic opal (Si_{OPAL})—from two sediment cores collected at 36°S off central Chile and covering the past 22 thousand years (kyr) (site PC-1), and at 52°S near the Pacific entrance of the Strait of Magellan and encompassing the past 13 kyr (site PC-3). During 13–8 calendar kyr before present (cal kyr BP), the ^{230}Th-normalized TOC flux at the PC-1 site was relatively high, pointing to increased productivity, whereas a marked decrease in the flux characterized the periods around 22–14 and 8–5 cal kyr BP. In contrast, at the PC-3 site, the ^{230}Th-normalized TOC flux was low during the last deglaciation until ~6 cal kyr BP, and then abruptly increased in the late Holocene. The ^{230}Th-normalized fluxes suggest that, compared to other periods, the biological pump functioned less effectively during 22–14 cal kyr BP and the middle Holocene off central Chile, and during 13–6 cal kyr BP off southernmost Patagonia. The changes from glacial to interglacial in the ^{230}Th-normalized biogenic components, which were controlled by changes in upwelling intensity at the PC-1 site and by the inflow of nutrients from the Pacific at the PC-3 site, can be explained by changes in wind direction and intensity associated with the latitudinal displacement of the southern westerly belt. In contrast, we found no obvious relationship during the deglacial and Holocene periods between El Niño activity and biogenic component fluxes at the PC-1 site, even though at present El Niño events are negatively correlated with primary productivity in the upwelling area off Chile.

Keywords: biological pump, paleoproductivity, thorium 230 (^{230}Th), southern westerlies, Chile

INTRODUCTION

Photosynthesis by phytoplankton plays an important role in the absorption of CO_2 from the atmosphere, and organic particles produced by phytoplankton effectively transport carbon to the deep-sea floor (e.g., Kawakami and Honda, 2007). Throughout geologic time, biogeochemical (e.g., export flux, nutrient utilization) and physical processes (e.g., upwelling, stratification) have together controlled the atmospheric partial pressure of CO_2 ($pCO_{2\,atm}$) (François *et al.*, 1997). With regard to the response of $pCO_{2\,atm}$ to global climate changes, one of the most important areas linking the atmosphere and the ocean is the Southern Ocean (François *et al.*, 1997; Anderson *et al.*, 2009; Sigman *et al.*, 2010), where upwelling of deep water brings carbon from one of the world's largest carbon reservoirs directly to the atmosphere. During glacial periods, strengthened productivity and an efficient biological pump in the North Pacific, equatorial Pacific, and Southern oceans may have contributed to low $pCO_{2\,atm}$ values (Broecker, 1982; McElroy,

*Corresponding author (e-mail: mh_fukud@geol.tsukuba.ac.jp)

1983; Martin, 1990; Kohfeld *et al*., 2005). However, whether marine productivity was high everywhere during glacial periods, especially during the Last Glacial Maximum (LGM: 26.5–19 cal kyr BP; Clark *et al*., 2009), is still controversial (e.g., Loubere *et al*., 2004). Resolving this controversy requires more data on temporal changes in past export fluxes of biogenic materials, especially from the eastern South Pacific Ocean, where active biological production is observed at present (Conkright *et al*., 1994).

Over the past two decades, many studies have examined paleoceanographic changes and the history of productivity in the Peru–Chile Current system. On a glacial–interglacial time scale, primary productivity in the upwelling ecosystem off northern Chile has varied with the precessional cycle (~20 kyr) and with inputs of iron from the continent, which vary with changes in precipitation (Dezileau *et al*., 2004). Paleoproductivity at 33°S off Chile was higher during the LGM than during the Holocene (11.5 cal kyr BP to the present; Mayewski *et al*., 2004). The Antarctic Circumpolar Current (ACC) was the main nutrient source during the LGM in this region (Hebbeln *et al*., 2002), and the southern westerly winds (SWW) generally carried large amounts of moisture. Therefore, shifts of the SWW increased onshore precipitation, thereby enhancing the nutrient supply to the Chilean coastal region (Mohtadi and Hebbeln, 2004). In contrast, productivity was low at 36°S during the LGM (Mohtadi *et al*., 2008), which has been explained by the northerly position of the SWW blowing directly onshore thus preventing coastal upwelling and export production off Concepción (Mohtadi *et al*., 2008) and a reduction of ACC nutrient levels caused by increased nitrate consumption in the subantarctic (Robinson *et al*., 2005). In this area, a rise in paleoproductivity at 13–14 cal kyr BP coincided with flooding of the shelf during Meltwater Pulse 1a and a strengthening of coastal upwelling, along with the southward migration of the SWW providing additional nutrients from the underlying Peru–Chile Undercurrent (PCU; Mohtadi *et al*., 2008). For southernmost Patagonia, Kilian *et al*. (2007) inferred a gradual increase of salinity and marine productivity between 14.5 and 13.5 cal kyr BP on the basis of an increase in the content of biogenic components and the first appearance of foraminifera in sediments. These phenomena imply that the deglacial marine transgression began at that time.

Most studies of paleoproductivity reconstructions off Chile, with the exception of one by Dezileau *et al*. (2004), have used mass accumulation rates (MAR) to represent changes in the relative contents of specific biogenic components (e.g., Mohtadi and Hebbeln, 2004; Romero *et al*., 2006). MAR, however, is not always the best proxy for productivity because of shortcomings in the MAR method: (1) the temporal resolution that can be obtained by this method is limited by the need to use the difference between two measured ages; (2) to calculate MAR, it is necessary to know the dry bulk density of the sediment; and (3) the method does not distinguish between contributions from vertical fluxes and those from lateral fluxes (François, 2007). Investigations from a different perspective (i.e., using a different proxy) are necessary to determine more accurately the paleo-fluxes of biogenic particles. In contrast, the ^{230}Th-normalization method corrects for sediment redistribution processes (focusing and winnowing) (Bacon, 1984). Thorium is highly insoluble in seawater, and ^{230}Th produced by the decay of dissolved ^{234}U is promptly removed from the water column by adsorption onto settling particles (Bacon and Anderson, 1982). The ^{230}Th-normalization method is based on the assumption that the flux of scavenged ^{230}Th reaching the seafloor is known and equal to the rate of ^{230}Th production from the decay of ^{234}U in the overlying water column. The ^{230}Th-normalization method greatly improves estimates of the export flux, although problems in resolution caused by bioturbation and preservation remain (François *et al*., 2004). Lyle *et al*. (2005, 2007) pointed out that one disadvantage of the ^{230}Th-normalization method is that it overestimates sediment focusing in the equatorial Pacific. In addition, independent information is required to assess horizontal sediment focusing, such as the characteristics of the source material, including the size of the source region, its sediment composition, and the degree of winnowing (Lyle *et al*., 2007). There is considerable lateral ^{230}Th input into the Pacific sector of the Southern Ocean from upwelling at higher latitudes along the ACC polar front (François *et al*., 2004), whereas the lateral addition of ^{230}Th from upwelling in the ACC is probably balanced by an equatorward export, resulting in scavenged ^{230}Th fluxes similar to the production rate, at least in the region along 170°W in the South Pacific (Chase *et al*., 2003). Thus, we believe that the use of this method to estimate the export flux in the South Pacific is justified.

The aim of this study was to examine changes in the ^{230}Th-normalized export fluxes of biogenic components commonly used as proxies for paleoproductivity—namely total organic carbon (TOC), total nitrogen (TN), calcium carbonate ($CaCO_3$), and biogenic opal (Si_{OPAL})—as recorded in sediment cores PC-1, from 36°S off the central Chilean coast, and PC-3, collected near the Pacific entrance of the Strait of Magellan (53°S). We compared our paleo-flux data with previously reported accumulation rates corrected for sediment redistribution by ^{230}Th-normalization in sediment cores from 27°S off northern Chile (Dezileau *et al*., 2004). Then, on the basis of this data set, we examined possible mechanisms underlying changes in primary production in the Chilean coastal area.

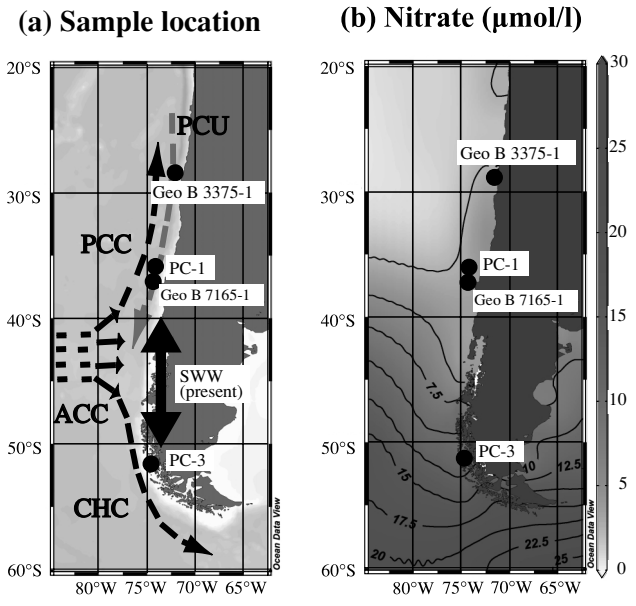

Fig. 1. (a) Sampling location of sediment cores PC-1 off central Chile (36°13′S, 73°41′W; 1022 m water depth) and PC-3 off southernmost Patagonia (52°52′S, 74°05′W; 560 m water depth), and major present-day currents. The positions of cores GeoB7165-1 (36°33′S, 73°40′W; 797 m water depth; Mohtadi et al., 2008) and GeoB3375-1 (27°28′S, 71°15′W; 1947 m water depth; Dezileau et al., 2004) are also shown since they are discussed in the text. The present predominant position and seasonal migration range of the southern westerly wind belt (SWW) are shown. (b) Nitrate distribution in surface waters. Currents in (a): ACC, Antarctic Circumpolar Current; PCU, Peru–Chile Undercurrent; PCC, Peru–Chile Current; CHC, Cape Horn Current. Data for (b) is from the World Ocean Atlas 2009, available from the NOAA National Ocean Data Center (http://www.nodc.noaa.gov/OC5/SELECT/woaselect/woaselect.html).

Study Area

The PC-1 site is located off the coast of central Chile (36° S; Fig. 1), where the strongest upwelling events occur in austral spring–summer and downwelling occurs in winter, when northerly winds prevail. Upwelled waters in this area commonly originate from the nutrient-rich Equatorial Subsurface Water (ESSW) mass, which is transported from north to south along the continental slope by the PCU (Fig. 1). Upwelling also results in a shallowing of the oxygen minimum zone, a feature linked to the ESSW (Strub *et al.*, 1998). On a seasonal time scale, subantarctic waters are dominant in the austral winter, when the winds are from the north, whereas in spring, summer, and early autumn, when south and southwesterly winds prevail, the ESSW upwells (e.g., Ahumada *et al.*, 1983). Primary production around the PC-1 site is 0.02–8 gC m^{-2} day^{-1} (Daneri *et al.*, 2000; Montecino *et al.*, 2004; Iriarte *et al.*, 2007) and can reach values of >20 gC m^{-2} day^{-1} on the shelf (e.g., Montero *et al.*, 2007), compared with 0.1–12 gC m^{-2} day^{-1} off Peru (Fernández *et al.*, 2009; Messié *et al.*, 2009). The area off 36° S also receives contributions from two major rivers, the Itata and the Bio-Bio. Precipitation and river discharge reduce the salinity of the upper 20 m of the water column, particularly in winter (Sobarzo *et al.*, 2007). These rivers also supply nutrients to the study area derived from weathered rocks of the Andes and the Coastal Range (Pineda, 1999).

The PC-3 site is located near the Pacific entrance of the Strait of Magellan (Fig. 1), ~5° north of the present-day Subantarctic Front (Orsi *et al.*, 1995). In southernmost Patagonia, surface oceanography is dominated by the Cape Horn Current (CHC), a coastal branch of the ACC (Strub *et al.*, 1998; Antezana, 1999; Chaigneau and Pizarro, 2005) (Fig. 1). The CHC flows poleward along the southernmost Chilean continental margin toward the Drake Passage and transports Subantarctic Surface Water (Shaffer *et al.*, 1995; Strub *et al.*, 1998). In the southern Chilean fjord region, the relatively saltier Pacific waters progressively mix with fresher waters derived from melting glaciers, precipitation, and river runoff to produce a positive estuarine circulation characterized by strong density, temperature, and salinity gradients (Pickard, 1971; Silva and Calvete, 2002; Sievers and Silva, 2008). However, the exchange between Magellan fjord waters and open Pacific water masses is somewhat restricted because of the shallow sill depth near Cabo Pilar at the western entrance of the Strait of Magellan (30–40 m; Antezana, 1999). The highest productivity season is from austral spring to early summer (Magazzù *et al.*, 1996; Oyarzrum *et al.*, 1999) with production values of 0.1–1.7 gC m^{-2} day^{-1} (Aracena *et al.*, 2011).

Materials and Methods

Sediment cores

Sediment core PC-1 (766 cm long) was collected ~65 km offshore of Concepción, Chile (36°13′ S, 73°41′ W; 1022 m water depth; Fig. 1). The sediments are characterized by homogeneous clayey silt/silty clay (Harada *et al.*, 2005). Sediment core PC-3 (964 cm long) was collected near the Pacific entrance of the Strait of Magellan (52°52′ S, 74°05′ W; 560 m water depth; Fig. 1). The sediments consist of calcareous sandy mud containing abundant calcareous fossils, including foraminifera, pteropods, bivalves, echinoids, and bryozoa (Harada *et al.*, 2005). Both cores were collected during cruise MR03-K04 onboard R/V *Mirai*. Cores were cut onboard into 1-m sections, which were split in half. Discrete sediment samples were collected at 2.25-cm intervals with a 10-ml syringe. For radiocarbon and oxygen isotope analysis of

planktic foraminifera, the coarse fraction (particles >63 μm) was used.

Analysis of total carbon, TOC, total nitrogen, and Si_{OPAL}

For the analysis of biogenic materials, bulk sediment samples were freeze-dried and ground into a homogeneous powder with a mortar and pestle. A dry sediment sample weighing 10 to 20 mg was placed into a tin capsule for measurement of total carbon (TC) and total nitrogen (TN) contents or into a silver capsule for measurement of TOC content (weight percent [wt%] of dry sediment). The samples in silver capsules were decalcified with sconcentrated HCl vapor for 8 h and then neutralized in an atmosphere of granular NaOH in a dry-conditioning desiccator for a few days before analysis. The samples in both tin and silver capsules were analyzed with an elemental analyzer (CHN Analyzer 2400II; Perkin Elmer). The $CaCO_3$ content was calculated by multiplying the inorganic carbon content (determined by subtracting TOC from TC) by the ratio of the molecular weight of $CaCO_3$ (100) to the atomic weight of carbon (12), using the following equation (e.g., Hebbeln *et al*., 2002; Mohtadi and Hebbeln, 2004): $CaCO_3$ (%) = (TC – TOC) × (100/12). The analytical errors determined by measuring duplicate samples for TC, TOC, and TN were within 2%, 2%, and 6%, respectively. The Si_{OPAL} content was determined from freeze-dried sediment samples (25–200 mg; collected at 10-cm intervals) after sequential leaching using the method of Mortlock and Froelich (1989) and modified by Müller and Schneider (1993). A single extraction of silica was performed with an alkaline solution at 85°C for 6 h and the dissolved silicon concentration in the extract was measured by molybdate-blue spectrophotometry at 812 nm. The results are expressed as Si_{OPAL} (%) = 112.4 × (Cs/M), where Cs is the silica concentration in the sample (nM), M is the sample mass (mg), and 112.4 is the molecular weight of Si (28.09) × the extraction volume of NaOH (0.04 L) × 100.

Measurement of radiocarbon in planktic foraminifera

We constructed an age model for core PC-1 by using radiocarbon (^{14}C) dating of planktic foraminifera. Radiocarbon dating requires at least 20 mg of carbonate, but no single planktic foraminiferal species was abundant enough within each 2.25-cm-thick sediment section to provide this amount of carbonate. Therefore, tests (>150 μm fraction) of several species of planktic foraminifera (*Globigerina bulloides*, *Globorotalia inflata*, *Neogloboquadrina pachyderma* sinistral [sin.] and dextral [dex.]) were picked from each discrete sample. All specimens of these four planktic foraminifera from the entire sediment sample were then used for ^{14}C measurement (Table 1). For PC-3, tests of *Globigerina bulloides* (>150 μm fraction) were used for radiocarbon dating (Table 1).

Table 1. Age model of core PC-1 at 36°S and PC-3 at 52°S. AMS ^{14}C dates and conversion to calendar ages based on the planktonic foraminifera (Globigerina bulloides, Globorotalia inflata, Neogloboquadrina pachyderma sinistral (sin.) and N. pachyderma dextral (dex.) in core PC-1. AMS ^{14}C dates and conversion to calendar ages based on the planktonic foraminifera Globigerina bulloides in core PC-3

Core	Depth (cm)	^{14}C age (yr BP*)	^{14}C age error (1σ, yr)	Calendar age (cal yr BP**)	Calendar age error (1σ, yr)
PC1	20.9	2890	50	3040	80
	73.7	9360	60	10080	120
	252	13960	90	16820	90
	366	15620	110	18310	240
	463	17310	80	20340	90
	560	18470	140	21760	280
PC3	21.4	2750	50	2577	57
	91.7	4300	50	4618	52
	139	5240	40	5747	76
	205	6920	40	7475	46
	296	8320	50	9066	68
	396	8890	50	9760	104
	593	9810	60	10953	34
	796	10420	60	12068	179

**Years before present.*
***Calendar years before present.*

Planktic foraminiferal shells were reacted with phosphoric acid under vacuum, and the released CO_2 gas was collected in a liquid nitrogen trap and purified by using a mixture of methanol and liquid nitrogen. The purified CO_2 gas was reduced to graphite with H_2 gas in a reaction furnace (670°C, 2 h). The $^{14}C/^{12}C$ ratio in each graphite sample was then measured by acceleration mass spectrometry (AMS) (tandem model at the National Institute for Environmental Studies, Japan, or the compact AMS, NEC model 1.5SDH, at Paleo Lab Co., Ltd., Japan). The ^{14}C ages were calculated from the $^{14}C/^{12}C$ ratio using Libby's ^{14}C half-life model based on AD 1950 (Stuiver and Polach, 1977), and converted to calendar ages using CalPal-2007 software (Weninger *et al*., 2009). For PC-1, we used the reservoir age of 400 years generally reported for the area off the Chilean margin (Mohtadi *et al*., 2008). For PC-3, we used a reservoir age of 680 years, estimated from mollusks collected at Puerto Natales, Chile (51°42′ S, 72°39′ W; Ingram and Southon, 1996). We could not obtain a ^{14}C age for the top of either core because of insufficient foraminifera; the youngest ^{14}C age was determined at 20.9 cm and 21.4 cm core depth of PC-1 and PC-3, respectively.

Oxygen isotope ratio ($\delta^{18}O$) analysis

Oxygen isotope ratios in shells of the planktic foraminifer *G. bulloides* from PC-1 were measured with a MAT 252 mass spectrometer (Thermo Fisher Scientific

Inc.). About 10 individual shells were picked from each sample, cleaned in ethanol, and treated with phosphoric acid at a constant temperature of 75°C. The evolved CO_2 gas was used for measurement of the stable oxygen isotope ratio. The isotope ratio data are reported using the standard delta notation in per mil relative to Pee Dee Belemnite (PDB) based on the NBS-19 standard. The oxygen isotope analysis error was within 0.06‰. Oxygen isotope ratios were not measured in PC-3, because insufficient planktic foraminifera after ^{14}C analysis.

Analysis of ^{230}Th, ^{232}Th, ^{238}U, and ^{234}U

Freeze-dried bulk sediment samples were completely dissolved in a mixture of HNO_3, $HClO_4$, and HF (1:1:1 by volume) in the presence of ^{232}U (5 disintegrations per minutes: dpm) and ^{228}Th (5 dpm) as yield tracers. Purification of radionuclides was carried out with an anion-exchange resin (AG1-X8; Bio-Rad Laboratories Inc.). Radionuclides were electroplated and counted with an alpha counter (Octéte; Seiko EG&G Co. Ltd.) following previously published methods (Anderson and Fleer, 1982; Narita *et al*., 2003). Uncertainties for radionuclides are indicated as counting errors (1σ). The detailed calculations to determine the vertical flux of biogenic components by the ^{230}Th-normalization method are summarized in Supplementary Materials. For PC-1, the ^{230}Th-normalized fluxes of TOC, TN, $CaCO_3$, and Si_{OPAL} have estimated propagation errors of 9–43%, 11–43%, 11–57%, and 10–43%, respectively. For PC-3, the ^{230}Th-normalized fluxes of TOC, TN, and Si_{OPAL} have estimated propagation errors of 3–83%, 4–84%, and 4–84%, respectively (see details in Supplementary Materials).

Focusing factor

In this study, we assumed that the flux of scavenged ^{230}Th ($^{230}Th^{scav}$) to the seafloor corresponds to its production rate in the overlying water column and that particles settle through the water column and accumulate on the seafloor without significant redistribution. Under this assumption, the $^{230}Th^{scav}$ inventory in the sediment between two different core depths should match the production of ^{230}Th in the overlying column (P_{230}) integrated over the time of accumulation of the sediments in that depth interval, after correction for radioactive decay. Using this principle, Suman and Bacon (1989) defined a focusing factor (Ψ) that quantifies syndepositional sediment redistribution. $\Psi = 1$ indicates that sediments are unaffected by syndepositional redistribution; $\Psi > 1$ indicates lateral addition of ^{230}Th and associated sediment, resulting in ^{230}Th accumulation rates higher than the production rate in the overlying water column (i.e., sediment focusing); and $\Psi < 1$ indicates lateral removal of ^{230}Th and associated sediment, resulting in ^{230}Th accumulation rates lower than the production rate (i.e., sediment winnowing). For PC-1 and PC-3, the focusing factors have estimated propagation errors of 6–12%, 3–12%, respectively (see details in Supplementary Materials).

RESULTS

Age model

Six calendar ^{14}C ages obtained from planktic foraminifera revealed that core PC-1 recorded approximately the past 22 kyr of sedimentation (Table 1 and Fig. 2a). $\delta^{18}O$ of *G. bulloides* ranged from 0.9‰ to 3.7‰ (Supplementary Table S1 and Fig. 2a). Relatively heavy values prevailed during the LGM, and values became lighter after the start of the deglaciation. Because no *G. bulloides* shells were found in sediments between 0 and 117.7 cm depth in the core (0–11.5 cal kyr BP), we were unable to determine the $\delta^{18}O$ values of *G. bulloides* over this depth range. Therefore, we also show the $\delta^{18}O$ data for foraminifera from sediment core GeoB7165-1, collected nearby (Mohtadi *et al*., 2008). The linear sedimentation rate (LSR) changed drastically with time; relatively high rates during the LGM and early deglaciation (>40 cm kyr^{-1}) decreased rapidly during 17–10 cal kyr BP to less than 7.5 cm kyr^{-1} during the Holocene (Fig. 2a).

The age model for core PC-3, based on eight ^{14}C ages, showed that this core covered the time interval from approximately 13 cal kyr BP until 2.5 cal kyr BP, thus recording part of the deglaciation (17.5–11.5 cal kyr BP) and most of the Holocene (Table 1). In this core, the LSR was relatively high (>140 cm kyr^{-1}) during the deglaciation and early Holocene, but rapidly decreased to less than 60 cm kyr^{-1} by 8 cal kyr BP (Fig. 2b).

TOC, TN, $CaCO_3$, and Si_{OPAL} content

The TOC content at the PC-1 site varied between 0.7% and 2.1% (Table S1 and Fig. 3a). It gradually increased from the LGM until the late deglaciation, and then increased abruptly at around 12–10 cal kyr BP. Except for an abrupt drop at ~9 cal kyr BP, the TOC content gradually increased throughout the Holocene. The TN content ranged from 0.08% to 0.26% over the last 22 kyr (Table S1 and Fig. 3b), with a pattern similar to that of TOC. The ratio of organic C to N, which is an indicator of the organic material source (typical C/N ratios: marine primary producers, 5–7, Libes, 1992; terrestrial plants >20, Meyers, 1994, and references therein), fluctuated slightly between 7.7 and 10 during the LGM and the early deglaciation, and thereafter was stable in the Holocene (8–9; Table S1 and Fig. 3c). Organic material at the PC-1 site was thus dominantly from marine organisms throughout the past 22 kyr. The Si_{OPAL} content fluctuated between 5.8 and 9.1% during the LGM–deglaciation, whereas values were more stable (Table S1 and Fig. 3d). The $CaCO_3$ content was relatively high with large fluctuations

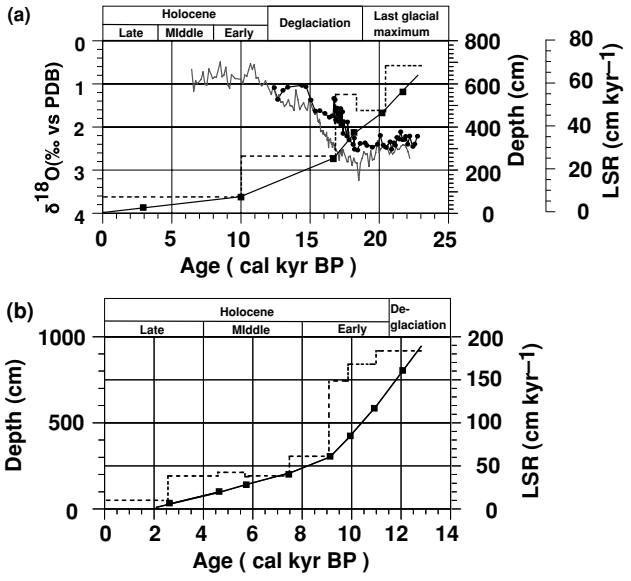

Fig. 2. (a) Stable oxygen isotope ratios in tests of Globigerina bulloides (filled black circles) in core PC-1 compared to $\delta^{18}O$ data derived from nearby sediment core GeoB7165-1 (gray line; data from Mohtadi et al., 2008). Filled squares and the solid black line indicate calendar ages converted from ^{14}C accelerator mass spectrometry (AMS) dates of planktic foraminifera by using CalPal-2007 software (see Table 1). The dashed line indicates the linear sedimentation rate (LSR) in relation to calendar age. (b) Calendar ages converted from ^{14}C AMS dates of planktic foraminifera by using CalPal-2007 software in core PC-3 (filled squares and solid line) (see Table 1). The dashed line indicates the LSR in relation to calendar age.

throughout the LGM and the deglaciation (mostly between 2 and 5%), but thereafter it gradually decreased, reaching very low values during the Holocene (Table S1 and Fig. 3e).

Although the water depth at the PC-1 site (1022 m) is much shallower than the $CaCO_3$ compensation depth (about 4500 m), few or no planktic foraminifera were present in the Holocene sediments. Low carbonate content and the scarcity of foraminifer shells in Holocene sediments seems to be a general feature in this region (Mohtadi and Hebbeln, 2004; Mohtadi *et al*., 2008).

At the PC-3 site, TOC varied between 0.4% and 1.6% (Supplementary Table S2 and Fig. 3a); it was relatively low from the late deglaciation until the early Holocene (13–8 cal kyr BP), increased abruptly at *ca*. 8 cal kyr BP, and then continued the increasing trend until the top of the core. The TN content ranged from 0.04% to 0.2% over the last 13 kyr (Table S2 and Fig. 3b) and increased in a pattern similar to that of TOC. The C/N ratio showed large fluctuations from 7.5 to 22 during 13–8 cal kyr BP (Table S2 and Fig. 3c), and thereafter the fluctuations became smaller and the ratio gradually decreased. For this site

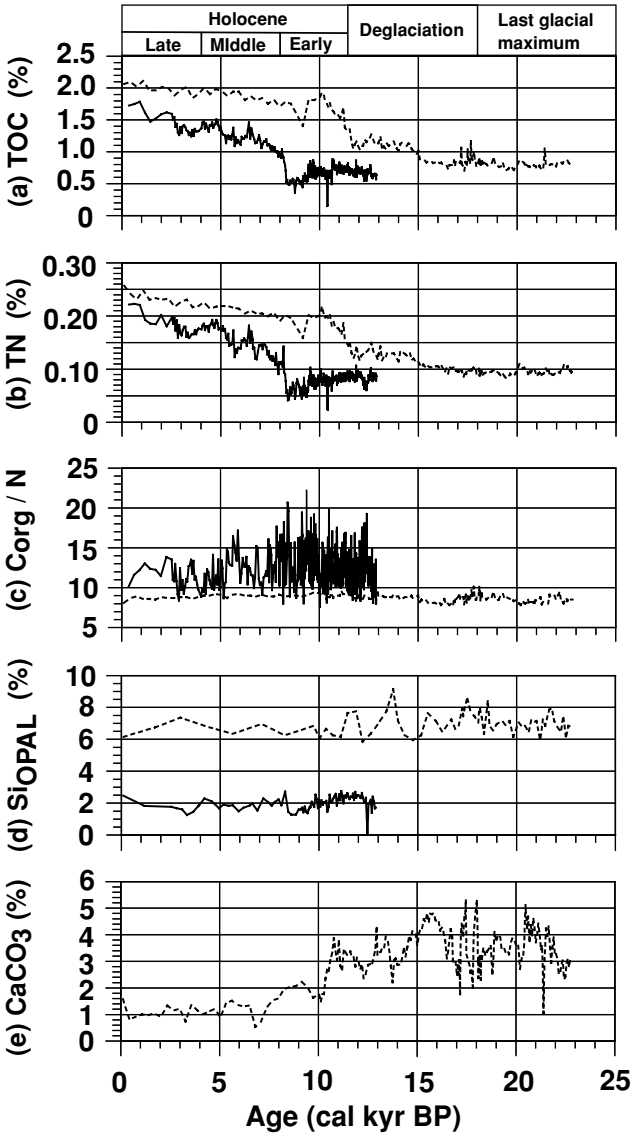

Fig. 3. Contents (% dry weight) of biogenic components and the ratio of organic carbon to nitrogen (w/w) in PC-1 (dashed lines, a–e) and PC-3 (solid lines, a–d): (a) TOC, (b) TN, (c) $C_{org.}/N$, (d) Si_{OPAL}, and (e) $CaCO_3$.

we assume an important contribution from terrigenous organic material, especially from 13 to 8 cal kyr BP. The Si_{OPAL} content at site PC-3 was much lower than that at site PC-1 and ranged from 1.2% to 2.7% over the last 13 kyr (Table S2 and Fig. 3d).

^{230}Th-normalized fluxes of TOC, $CaCO_3$, and Si_{OPAL}

The overall range of ^{230}Th-normalized fluxes of TOC at the PC-1 site was 10 to 49 mg cm^{-2} kyr^{-1} (Table 2 and Fig. 4a). Values were low during 22–14 cal kyr BP and 8–5 cal kyr BP and highest (>40 mg cm^{-2} kyr^{-1}) at 13–10 cal kyr BP and in the past 3,000 years. The ^{230}Th-

normalized fluxes of $CaCO_3$ showed a different pattern with relatively high values during the LGM and the deglaciation (46 to 107 mg cm^{-2} kyr^{-1}; Table 2 and Fig. 4b) and low Holocene fluxes ranging from 14 to 45 mg cm^{-2} kyr^{-1}. The ^{230}Th-normalized fluxes of Si_{OPAL} fluctuated widely throughout the past 22 kyr, with values ranging between 93 mg cm^{-2} kyr^{-1} in the middle Holocene and 231 mg cm^{-2} kyr^{-1} at 13.0 cal kyr BP (Table 2 and Fig. 4c).

In contrast to the PC-1 patterns, the ^{230}Th-normalized fluxes of TOC at the PC-3 site ranged from 5.1 to 159 mg cm^{-2} kyr^{-1} (Table 2 and Fig. 4a) with relatively low values during 13–6 cal kyr BP, and increasing rapidly at ~5 cal kyr BP toward the top of the core. The ^{230}Th-normalized fluxes of Si_{OPAL} ranged from 8.1 to 184 mg cm^{-2} kyr^{-1} (Table 2 and Fig. 4c). Relatively high values (>100 mg cm^{-2} kyr^{-1}) were observed between 13 and 11 cal kyr BP, at 9–8 cal kyr BP, and in sediments younger than 5 cal kyr BP. At all times, Si_{OPAL} fluxes at the PC-3 site were no more than one-third of those at the PC-1 site, except at around 5 cal kyr BP. Harada *et al*. (2012) showed that the ^{230}Th-normalized method is valid for the estimation of the biological fluxes in these sediment core because the estimation of the biological fluxes were comparable with those derived from MAR method.

Focusing factor

A focusing factor was calculated using the activity of scavenged ^{230}Th and the initial activity of the scavenged ^{230}Th (Table 2). At the PC-1 site, the focusing factor varied from 3.2 to 29; it was fairly high during the LGM and then it decreased toward the Holocene (Fig. 4d). At the PC-3 site, the focusing factor varied between 5.9 and 67; it was high during 13–9 cal kyr BP, it dropped at 8–6 cal kyr BP, and then it again became high during 5–3 cal kyr BP (Fig. 4d). Values >1 throughout the past 22 kyr at the PC-1 site and the past 13 kyr at the PC-3 site suggest that the Chilean coastal region is a sediment focusing region. Overall changes in the focusing factor at both sites were similar to the changes in the LSRs (Fig. 2), suggesting that sediment focusing was intensified during the LGM and the last deglaciation.

Discussion

Changes in productivity off central-south Chile and southernmost Patagonia

The ^{230}Th-normalized fluxes of TOC that we observed at the PC-1 site during the LGM (low values, ~30 mg cm^{-2} kyr^{-1}) are consistent with the paleoproductivity pattern reported by Mohtadi *et al*. (2008) for the nearby core site GeoB7165-1 but differ from the estimated MARs of TOC and Si_{OPAL} at ODP sites 1234 and 1235 off Concepción (at 1015 m and 489 m water depth, respectively). At the ODP sites, the TOC and Si_{OPAL} MARs were higher during the glacial and deglacial periods (30–15 cal kyr BP) than at any other time over the past 30 kyr (Muratli *et al*., 2010). Higher paleoproductivity during the LGM based on the MARs of biogenic components has been reported previously off the Chilean coast at 33°S and 35°S (Lamy *et al*., 1999; Hebbeln *et al*., 2002; Mohtadi and Hebbeln, 2004; Romero *et al*., 2006), whereas north of 33°S, productivity was higher prior to the LGM and during the postglacial than during other periods (Mohtadi and Hebbeln, 2004). As indicated by our focusing factor at the PC-1 site, sediment focusing was stronger during the LGM than during the deglaciation or the Holocene (Fig. 4d). This result suggests that the high TOC and Si_{OPAL} MARs at ODP sites 1234 and 1235 off Concepción during the LGM might have been caused by high LSR rather than productivity. Although the record of core GeoB7165-1, near the PC-1 site, includes no information on sediments younger than 6 cal kyr BP (Mohtadi *et al*., 2008), in that core some paleoproductivity proxies show decreases at ~6–8 cal kyr BP. In addition, foraminiferal records from ~33°S off Valparaiso suggest reduced upwelling and low productivity between 10 and ~3 cal kyr BP (Marchant *et al*., 1999).

To the best of our knowledge, the only other study off Chile using ^{230}Th-normalized values of TOC, $CaCO_3$, biogenic opal, and iron is the one by Dezileau *et al*. (2004). They found that at GeoB3375-1 (27°S), in the upwelling area off northern Chile, productivity was higher during the LGM than during the deglaciation (Fig. 4). From the LGM to 14 cal kyr BP, ^{230}Th-normalized fluxes of TOC at the PC-1 site were similar or slightly lower than those at the GeoB3375-1 site, whereas from 14 to 10 cal kyr BP they were much higher, not only at the PC-1 site but also at the PC-3 site (Fig. 4a). On the other hand, ^{230}Th-normalized fluxes of $CaCO_3$ were consistently one order of magnitude higher in GeoB3375-1 than in PC-1; at both sites the highest values occurred during the LGM, and then the fluxes gradually decreased toward the Holocene. When comparing ^{230}Th-normalized fluxes of Si_{OPAL}, site GeoB3375-1 showed higher values during the LGM than during other periods; however, fluxes throughout the record were always lower than those recorded at the PC-1 and PC-3 sites. In fact, fluxes at the PC-1 site were both highest and very variable and a clear trend could not be discerned.

If we assume that ^{230}Th-normalized accumulation rates represent the flux of material from the water column directly above each coring site (e.g., François *et al*., 2004), then the temporal and spatial changes in the paleo-export fluxes of biogenic components at 27°S, 36°S and 52°S off the Chilean coast imply that the biological pump was (i) effective during the LGM off northern Chile, during 14–8 cal kyr BP off central Chile, and after 5 cal kyr BP off central and southernmost Chile; and (ii) not fully ef-

Table 2. Activities of ^{230}Th, ^{232}Th, ^{238}U and ^{230}Th-normalized fluxes of total organic carbon, total nitrogen, $CaCO_3$, Si_{OPAL} in core PC-1 and PC-3

Core	Depth (cm)	Age (cal kyr BP)	Water depth (m)	Activity of total ^{230}Th (dpm g^{-1})	Activity of total ^{232}Th (dpm g^{-1})	Activity of detrital ^{230}Th (dpm g^{-1})	Activity of total ^{238}U (dpm g^{-1})	Activity of authigenic ^{230}Th (dpm g^{-1})
PC1	9.90	1.44 ± 0.080	1021	1.5 ± 0.062	1.0 ± 0.044	0.38 ± 0.097	3.8 ± 0.17	0.050 ± 0.0040
	20.9	3.04 ± 0.080	1018	1.9 ± 0.086	1.7 ± 0.080	0.69 ± 0.18	3.1 ± 0.14	0.075 ± 0.0073
	36.3	5.09 ± 0.080	1013	2.4 ± 0.13	1.9 ± 0.11	0.76 ± 0.20	1.8 ± 0.082	0.055 ± 0.011
	56.1	7.73 ± 0.080	1011	3.5 ± 0.39	3.4 ± 0.39	1.4 ± 0.38	7.6 ± 0.37	0.48 ± 0.041
	73.7	10.1 ± 0.12	978	1.7 ± 0.066	1.4 ± 0.055	0.54 ± 0.14	2.8 ± 0.12	0.23 ± 0.019
	152	13.0 ± 0.12	950	1.2 ± 0.053	0.82 ± 0.040	0.33 ± 0.083	1.9 ± 0.075	0.21 ± 0.014
	189	14.5 ± 0.090	923	2.1 ± 0.12	1.9 ± 0.11	0.75 ± 0.19	1.7 ± 0.056	0.13 ± 0.028
	211	15.3 ± 0.12	913	1.4 ± 0.066	0.82 ± 0.043	0.33 ± 0.08	1.8 ± 0.075	0.22 ± 0.017
	252	16.8 ± 0.090	905	1.6 ± 0.073	1.4 ± 0.064	0.55 ± 0.14	1.5 ± 0.074	0.16 ± 0.026
	267	17.0 ± 0.090	904	1.6 ± 0.079	1.4 ± 0.072	0.58 ± 0.15	1.9 ± 0.071	0.22 ± 0.027
	304	17.8 ± 0.090	901	1.6 ± 0.078	0.91 ± 0.050	0.36 ± 0.093	2.7 ± 0.10	0.40 ± 0.023
	322	18.1 ± 0.090	900	1.7 ± 0.069	1.3 ± 0.056	0.53 ± 0.13	2.7 ± 0.12	0.38 ± 0.031
	366	18.3 ± 0.24	898	1.9 ± 0.10	1.8 ± 0.093	0.73 ± 0.19	2.8 ± 0.13	0.37 ± 0.040
	428	19.6 ± 0.24	885	2.3 ± 0.12	1.2 ± 0.070	0.49 ± 0.13	2.4 ± 0.10	0.36 ± 0.030
	463	20.3 ± 0.090	884	1.8 ± 0.078	1.5 ± 0.067	0.60 ± 0.15	2.0 ± 0.10	0.28 ± 0.035
	511	21.1 ± 0.090	884	1.9 ± 0.10	1.1 ± 0.065	0.46 ± 0.12	2.8 ± 0.12	0.48 ± 0.033
	561	21.8 ± 0.28	884	1.8 ± 0.070	2.0 ± 0.076	0.80 ± 0.20	1.6 ± 0.073	0.17 ± 0.044
	612	22.5 ± 0.28	884	1.6 ± 0.081	1.0 ± 0.056	0.39 ± 0.10	2.8 ± 0.10	0.52 ± 0.031
PC3	21.4	2.31 ± 0.057	558	0.51 ± 0.019	0.55 ± 0.021	0.22 ± 0.056	3.8 ± 0.14	0.086 ± 0.0041
	32.6	2.88 ± 0.057	557	0.52 ± 0.021	0.58 ± 0.023	0.23 ± 0.059	3.5 ± 0.14	0.097 ± 0.0048
	41.6	3.13 ± 0.052	557	0.54 ± 0.022	0.56 ± 0.022	0.23 ± 0.057	3.6 ± 0.13	0.11 ± 0.0048
	52.9	3.44 ± 0.052	557	0.49 ± 0.020	0.61 ± 0.023	0.24 ± 0.061	4.0 ± 0.15	0.13 ± 0.0059
	61.9	3.68 ± 0.052	557	0.53 ± 0.021	0.54 ± 0.021	0.21 ± 0.054	3.9 ± 0.17	0.14 ± 0.0070
	70.9	3.93 ± 0.052	556	0.57 ± 0.020	0.62 ± 0.021	0.25 ± 0.062	4.5 ± 0.15	0.17 ± 0.0068
	91.7	4.50 ± 0.052	556	1.4 ± 0.023	1.4 ± 0.022	0.55 ± 0.14	4.0 ± 0.14	0.16 ± 0.0092
	98.5	4.67 ± 0.076	556	0.59 ± 0.055	0.54 ± 0.024	0.22 ± 0.055	4.3 ± 0.15	0.20 ± 0.0083
	105	4.83 ± 0.076	556	3.6 ± 0.17	3.2 ± 0.16	1.3 ± 0.33	7.0 ± 0.30	0.28 ± 0.022
	114	5.05 ± 0.076	555	0.57 ± 0.025	0.56 ± 0.024	0.22 ± 0.056	4.3 ± 0.18	0.21 ± 0.010
	125	5.32 ± 0.076	555	5.6 ± 0.61	5.6 ± 0.61	2.3 ± 0.61	7.5 ± 0.22	0.28 ± 0.035
	143	5.75 ± 0.076	555	0.68 ± 0.029	0.64 ± 0.028	0.26 ± 0.065	4.4 ± 0.19	0.24 ± 0.012
	152	5.99 ± 0.046	554	1.5 ± 0.053	1.5 ± 0.053	0.61 ± 0.15	6.3 ± 0.18	0.35 ± 0.015
	185	6.86 ± 0.046	554	1.6 ± 0.068	1.5 ± 0.063	0.59 ± 0.15	6.2 ± 0.19	0.39 ± 0.017
	209	7.51 ± 0.068	550	1.5 ± 0.072	1.7 ± 0.077	0.67 ± 0.17	5.8 ± 0.21	0.39 ± 0.021
	230	7.85 ± 0.068	548	1.3 ± 0.054	1.5 ± 0.059	0.60 ± 0.15	3.7 ± 0.12	0.24 ± 0.015
	254	8.26 ± 0.068	545	0.62 ± 0.028	0.87 ± 0.036	0.35 ± 0.088	1.0 ± 0.033	0.057 ± 0.008

Core	Depth (cm)	Age (cal kyr BP)	Water depth (m)	Activity of total ^{230}Th (dpm g^{-1})	Activity of total ^{232}Th (dpm g^{-1})	Activity of detrital ^{230}Th (dpm g^{-1})	Activity of total ^{238}U (dpm g^{-1})	Activity of authigenic ^{230}Th (dpm g^{-1})
PC3	272	8.56 ± 0.068	541	0.85 ± 0.034	1.2 ± 0.043	0.47 ± 0.12	2.4 ± 0.10	0.16 ± 0.013
	287	8.80 ± 0.068	540	1.0 ± 0.028	1.3 ± 0.037	0.53 ± 0.13	2.0 ± 0.082	0.13 ± 0.014
	298	8.99 ± 0.068	535	0.57 ± 0.026	0.77 ± 0.033	0.31 ± 0.079	1.3 ± 0.053	0.090 ± 0.009
	312	9.13 ± 0.10	533	1.1 ± 0.031	1.2 ± 0.034	0.49 ± 0.12	2.5 ± 0.072	0.18 ± 0.013
	332	9.27 ± 0.10	530	1.3 ± 0.047	1.5 ± 0.052	0.60 ± 0.15	1.9 ± 0.055	0.12 ± 0.015
	375	9.56 ± 0.10	526	1.2 ± 0.047	1.7 ± 0.061	0.68 ± 0.17	1.5 ± 0.044	0.074 ± 0.017
	387	9.64 ± 0.10	525	1.0 ± 0.023	1.4 ± 0.033	0.58 ± 0.14	1.8 ± 0.053	0.12 ± 0.015
	412	9.80 ± 0.034	522	1.0 ± 0.034	1.3 ± 0.040	0.51 ± 0.13	1.4 ± 0.039	0.086 ± 0.013
	432	9.93 ± 0.034	519	0.88 ± 0.026	1.1 ± 0.032	0.44 ± 0.11	1.6 ± 0.045	0.11 ± 0.012
	475	10.2 ± 0.034	514	0.92 ± 0.023	1.3 ± 0.031	0.51 ± 0.13	1.4 ± 0.045	0.10 ± 0.014
	486	10.3 ± 0.034	512	0.83 ± 0.029	1.1 ± 0.037	0.44 ± 0.11	1.4 ± 0.049	0.093 ± 0.013
	511	10.4 ± 0.034	509	0.93 ± 0.039	1.5 ± 0.057	0.61 ± 0.15	1.3 ± 0.047	0.071 ± 0.017
	531	10.5 ± 0.034	508	0.81 ± 0.031	1.1 ± 0.039	0.45 ± 0.11	1.1 ± 0.046	0.073 ± 0.013
	574	10.8 ± 0.034	505	1.0 ± 0.039	1.2 ± 0.045	0.47 ± 0.12	1.4 ± 0.050	0.10 ± 0.014
	586	10.9 ± 0.034	502	0.92 ± 0.038	1.2 ± 0.045	0.47 ± 0.12	1.4 ± 0.053	0.10 ± 0.014
	611	11.0 ± 0.18	502	1.3 ± 0.049	1.5 ± 0.057	0.61 ± 0.15	1.5 ± 0.033	0.091 ± 0.017
	631	11.1 ± 0.18	501	1.0 ± 0.032	1.4 ± 0.043	0.55 ± 0.14	1.3 ± 0.030	0.084 ± 0.016
	652	11.2 ± 0.18	499	0.67 ± 0.027	1.0 ± 0.038	0.42 ± 0.11	0.94 ± 0.030	0.058 ± 0.012
	672	11.3 ± 0.18	498	1.0 ± 0.031	1.2 ± 0.035	0.47 ± 0.12	1.4 ± 0.059	0.11 ± 0.015
	685	11.4 ± 0.18	497	0.63 ± 0.025	0.91 ± 0.032	0.36 ± 0.092	0.89 ± 0.033	0.060 ± 0.011
	703	11.5 ± 0.18	496	1.0 ± 0.036	1.3 ± 0.046	0.53 ± 0.13	1.3 ± 0.045	0.087 ± 0.016
	717	11.6 ± 0.18	495	0.73 ± 0.030	0.81 ± 0.032	0.32 ± 0.082	0.94 ± 0.035	0.070 ± 0.010
	730	11.7 ± 0.18	495	0.60 ± 0.023	0.81 ± 0.028	0.32 ± 0.082	0.84 ± 0.028	0.059 ± 0.010
	748	11.8 ± 0.18	494	0.89 ± 0.035	1.1 ± 0.042	0.45 ± 0.11	1.3 ± 0.043	0.094 ± 0.014
	766	11.9 ± 0.18	494	0.63 ± 0.026	0.85 ± 0.032	0.34 ± 0.086	0.84 ± 0.033	0.058 ± 0.011
	793	12.0 ± 0.18	494	0.56 ± 0.023	0.83 ± 0.030	0.33 ± 0.084	0.84 ± 0.033	0.061 ± 0.011
	807	12.1 ± 0.18	493	1.0 ± 0.035	1.1 ± 0.039	0.44 ± 0.11	1.3 ± 0.049	0.10 ± 0.015
	829	12.2 ± 0.18	493	0.66 ± 0.024	0.91 ± 0.031	0.37 ± 0.092	0.90 ± 0.036	0.064 ± 0.012
	847	12.3 ± 0.18	492	0.58 ± 0.023	0.90 ± 0.031	0.36 ± 0.091	0.80 ± 0.031	0.053 ± 0.012
	865	12.4 ± 0.18	491	0.63 ± 0.025	0.78 ± 0.029	0.31 ± 0.078	0.88 ± 0.035	0.069 ± 0.011
	885	12.5 ± 0.18	491	0.72 ± 0.029	0.91 ± 0.034	0.36 ± 0.092	1.0 ± 0.037	0.074 ± 0.012
	894	12.6 ± 0.18	491	0.88 ± 0.036	1.0 ± 0.041	0.42 ± 0.11	1.2 ± 0.049	0.10 ± 0.015
	905	12.6 ± 0.18	490	0.60 ± 0.025	0.84 ± 0.031	0.34 ± 0.085	0.94 ± 0.037	0.075 ± 0.012
	921	12.7 ± 0.18	490	0.55 ± 0.022	0.86 ± 0.030	0.34 ± 0.086	0.77 ± 0.029	0.054 ± 0.011
	939	12.8 ± 0.18	489	0.69 ± 0.030	0.80 ± 0.033	0.32 ± 0.081	1.3 ± 0.042	0.13 ± 0.012
	961	12.9 ± 0.18	488	0.57 ± 0.022	0.79 ± 0.028	0.31 ± 0.079	0.80 ± 0.027	0.062 ± 0.011

Table 2. (continued)

Core	Activity of scavenged ^{230}Th (dpm g^{-1})	Initial activity of scavenged ^{230}Th (dpm g^{-1})	Preserved vertical flux (g cm^{-2} kyr^{-1})	Total org. C flux (mg cm^{-2} kyr^{-1})	$CaCO_3$ flux (mg cm^{-2} kyr^{-1})	Opal flux (mg cm^{-2} kyr^{-1})	Focusing factor ψ (Suman and Bacon, 1989)
PC1	1.1 ± 0.12	1.1 ± 0.12	2.5 ± 0.33	49 ± 6.5	24 ± 8.8	169 ± 24	3.2 ± 0.45
	1.1 ± 0.20	1.2 ± 0.20	2.4 ± 0.55	46 ± 11	28 ± 10	172 ± 41	
	1.6 ± 0.24	1.7 ± 0.25	1.6 ± 0.68	31 ± 13	14 ± 7.8	104 ± 45	
	1.6 ± 0.55	1.7 ± 0.59	1.6 ± 1.6	28 ± 29	24 ± 24	103 ± 104	
	0.90 ± 0.15	1.0 ± 0.17	2.6 ± 0.45	49 ± 8.4	45 ± 11	157 ± 28	10 ± 1.1
	0.67 ± 0.10	0.75 ± 0.12	3.4 ± 0.29	38 ± 3.4	107 ± 11	231 ± 23	
	1.2 ± 0.23	1.3 ± 0.26	1.8 ± 0.64	20 ± 7.0	58 ± 21	114 ± 40	
	0.88 ± 0.11	1.0 ± 0.13	2.4 ± 0.31	21 ± 2.8	101 ± 14	149 ± 21	
	0.93 ± 0.16	1.1 ± 0.19	2.2 ± 0.46	17 ± 3.6	86 ± 18	160 ± 34	
	0.82 ± 0.17	1.0 ± 0.20	2.5 ± 0.48	20 ± 3.9	71 ± 14	168 ± 33	21 ± 2.2
	0.84 ± 0.12	1.0 ± 0.15	2.4 ± 0.36	21 ± 3.1	66 ± 10	188 ± 29	
	0.81 ± 0.15	1.0 ± 0.18	2.5 ± 0.44	22 ± 3.8	101 ± 18	177 ± 32	
	0.85 ± 0.21	1.0 ± 0.26	2.4 ± 0.62	18 ± 4.8	72 ± 19	162 ± 43	
	1.5 ± 0.18	1.8 ± 0.23	1.3 ± 0.53	10 ± 3.8	46 ± 18	93 ± 37	27 ± 4.1
	0.89 ± 0.17	1.1 ± 0.21	2.2 ± 0.50	18 ± 4.1	68 ± 16	148 ± 34	
	1.0 ± 0.16	1.2 ± 0.19	2.0 ± 0.46	14 ± 3.2	74 ± 17	142 ± 33	29 ± 3.8
	0.85 ± 0.22	1.0 ± 0.27	2.3 ± 0.64	18 ± 5.1	83 ± 24	179 ± 51	
	0.72 ± 0.13	0.89 ± 0.17	2.7 ± 0.40	23 ± 3.4	63 ± 10	159 ± 25	
PC3	0.20 ± 0.059	0.20 ± 0.061	7.4 ± 0.090	117 ± 3.8		127 ± 6.5	5.9 ± 0.71
	0.19 ± 0.063	0.20 ± 0.064	7.5 ± 0.096	97 ± 3.2		123 ± 6.4	
	0.20 ± 0.061	0.21 ± 0.063	7.1 ± 0.094	99 ± 3.2		111 ± 5.7	
	0.11 ± 0.065	0.12 ± 0.067	13 ± 0.099	159 ± 4.9		153 ± 7.8	
	0.18 ± 0.059	0.18 ± 0.061	8.0 ± 0.090	100 ± 3.2		112 ± 5.8	
	0.16 ± 0.066	0.16 ± 0.068	9.2 ± 0.10	121 ± 3.9		161 ± 8.2	
	0.68 ± 0.14	0.71 ± 0.15	2.1 ± 0.22	29 ± 3.2		43 ± 4.9	
	0.18 ± 0.078	0.19 ± 0.082	7.9 ± 0.12	108 ± 3.6		162 ± 8.5	33 ± 5.6
	2.0 ± 0.37	2.1 ± 0.39	0.69 ± 0.58	10 ± 8.7		13 ± 11	
	0.14 ± 0.062	0.15 ± 0.066	10 ± 0.10	137 ± 4.3		162 ± 8.3	
	3.1 ± 0.863	3.3 ± 0.91	0.45 ± 1.3	5.1 ± 15		8.1 ± 24	
	0.18 ± 0.072	0.19 ± 0.08	7.6 ± 0.11	82 ± 2.7		138 ± 7.2	
	0.54 ± 0.16	0.57 ± 0.17	2.6 ± 0.26	29 ± 3.0		37 ± 4.2	18 ± 3.5
	0.66 ± 0.17	0.70 ± 0.18	2.1 ± 0.26	24 ± 3.0		31 ± 4.4	
	0.48 ± 0.19	0.52 ± 0.20	2.8 ± 0.29	31 ± 3.4		57 ± 6.5	18 ± 3.2
	0.48 ± 0.16	0.52 ± 0.17	2.8 ± 0.26	28 ± 2.7		57 ± 5.9	
	0.21 ± 0.09	0.23 ± 0.10	6.3 ± 0.15	52 ± 2.0		167 ± 9.2	

Core	Activity of scavenged ^{230}Th (dpm g^{-1})	Initial activity of scavenged ^{230}Th (dpm g^{-1})	Preserved vertical flux (g cm^{-2} kyr^{-1})	Total org. C flux (mg cm^{-2} kyr^{-1})	$CaCO_3$ flux (mg cm^{-2} kyr^{-1})	Opal flux (mg cm^{-2} kyr^{-1})	Focusing factor ψ (Suman and Bacon, 1989)
PC3	0.22 ± 0.12	0.24 ± 0.13	6.1 ± 0.19	33 ± 1.4		80 ± 5.0	
	0.32 ± 0.14	0.35 ± 0.15	4.1 ± 0.21	14 ± 0.86		50 ± 3.6	
	0.17 ± 0.083	0.19 ± 0.09	7.6 ± 0.13	41 ± 1.4		117 ± 6.2	
	0.43 ± 0.13	0.47 ± 0.14	3.0 ± 0.20	16 ± 1.2		47 ± 3.9	67 ± 12
	0.62 ± 0.16	0.67 ± 0.18	2.1 ± 0.25	12 ± 1.5		29 ± 3.8	
	0.44 ± 0.18	0.48 ± 0.20	2.9 ± 0.27	17 ± 1.7		47 ± 4.9	
	0.29 ± 0.15	0.32 ± 0.16	4.4 ± 0.23	34 ± 2.0		74 ± 5.3	
	0.43 ± 0.13	0.47 ± 0.15	3.0 ± 0.20	20 ± 1.5		51 ± 4.4	57 ± 7.9
	0.32 ± 0.12	0.35 ± 0.13	4.0 ± 0.18	29 ± 1.5		89 ± 6.3	
	0.31 ± 0.13	0.34 ± 0.14	4.0 ± 0.20	26 ± 1.5		85 ± 5.4	
	0.30 ± 0.12	0.33 ± 0.13	4.2 ± 0.18	30 ± 1.6		77 ± 5.5	
	0.25 ± 0.16	0.27 ± 0.18	5.0 ± 0.24	34 ± 2.0		104 ± 7.0	
	0.29 ± 0.12	0.32 ± 0.13	4.2 ± 0.18	25 ± 1.3		73 ± 4.2	
	0.39 ± 0.13	0.43 ± 0.14	3.1 ± 0.19	27 ± 1.8		70 ± 5.3	
	0.36 ± 0.12	0.40 ± 0.14	3.4 ± 0.18	25 ± 1.5		80 ± 5.8	
	0.55 ± 0.16	0.61 ± 0.18	2.2 ± 0.24	16 ± 1.8		48 ± 6.0	57 ± 4.8
	0.32 ± 0.14	0.36 ± 0.16	3.8 ± 0.21	27 ± 1.7		80 ± 6.1	
	0.19 ± 0.11	0.22 ± 0.12	6.2 ± 0.16	41 ± 1.6		148 ± 9.2	
	0.45 ± 0.12	0.50 ± 0.14	2.7 ± 0.18	20 ± 1.5		64 ± 5.5	
	0.21 ± 0.096	0.23 ± 0.11	5.8 ± 0.14	42 ± 1.6		136 ± 7.7	
	0.36 ± 0.14	0.40 ± 0.16	3.3 ± 0.21	24 ± 1.7		86 ± 6.6	
	0.33 ± 0.088	0.37 ± 0.099	3.6 ± 0.13	26 ± 1.2		78 ± 5.4	
	0.22 ± 0.085	0.25 ± 0.096	5.4 ± 0.13	37 ± 1.4		126 ± 6.6	
	0.34 ± 0.12	0.38 ± 0.13	3.5 ± 0.18	22 ± 1.3		88 ± 6.2	
	0.23 ± 0.091	0.25 ± 0.10	5.2 ± 0.13	37 ± 1.5		138 ± 7.4	
	0.17 ± 0.087	0.19 ± 0.098	7.1 ± 0.13	49 ± 1.7		171 ± 8.7	
	0.43 ± 0.12	0.48 ± 0.13	2.7 ± 0.17	18 ± 1.3		64 ± 5.2	
	0.23 ± 0.096	0.26 ± 0.11	5.1 ± 0.14	35 ± 1.4		132 ± 6.9	
	0.17 ± 0.094	0.19 ± 0.11	7.1 ± 0.14	38 ± 1.4		151 ± 9.7	
	0.25 ± 0.083	0.28 ± 0.094	4.7 ± 0.12	28 ± 1.1		99 ± 5.3	
	0.29 ± 0.097	0.32 ± 0.11	4.1 ± 0.14	26 ± 1.2		88 ± 5.1	
	0.36 ± 0.11	0.40 ± 0.13	3.3 ± 0.17	21 ± 1.3		62 ± 4.9	
	0.19 ± 0.089	0.22 ± 0.10	6.1 ± 0.13	47 ± 1.7		121 ± 7.2	
	0.15 ± 0.090	0.17 ± 0.10	7.6 ± 0.13	48 ± 1.6		101 ± 7.8	
	0.24 ± 0.087	0.27 ± 0.099	4.8 ± 0.13	29 ± 1.2		97 ± 4.1	
	0.19 ± 0.083	0.21 ± 0.094	6.1 ± 0.12	38 ± 1.4		101 ± 6.4	

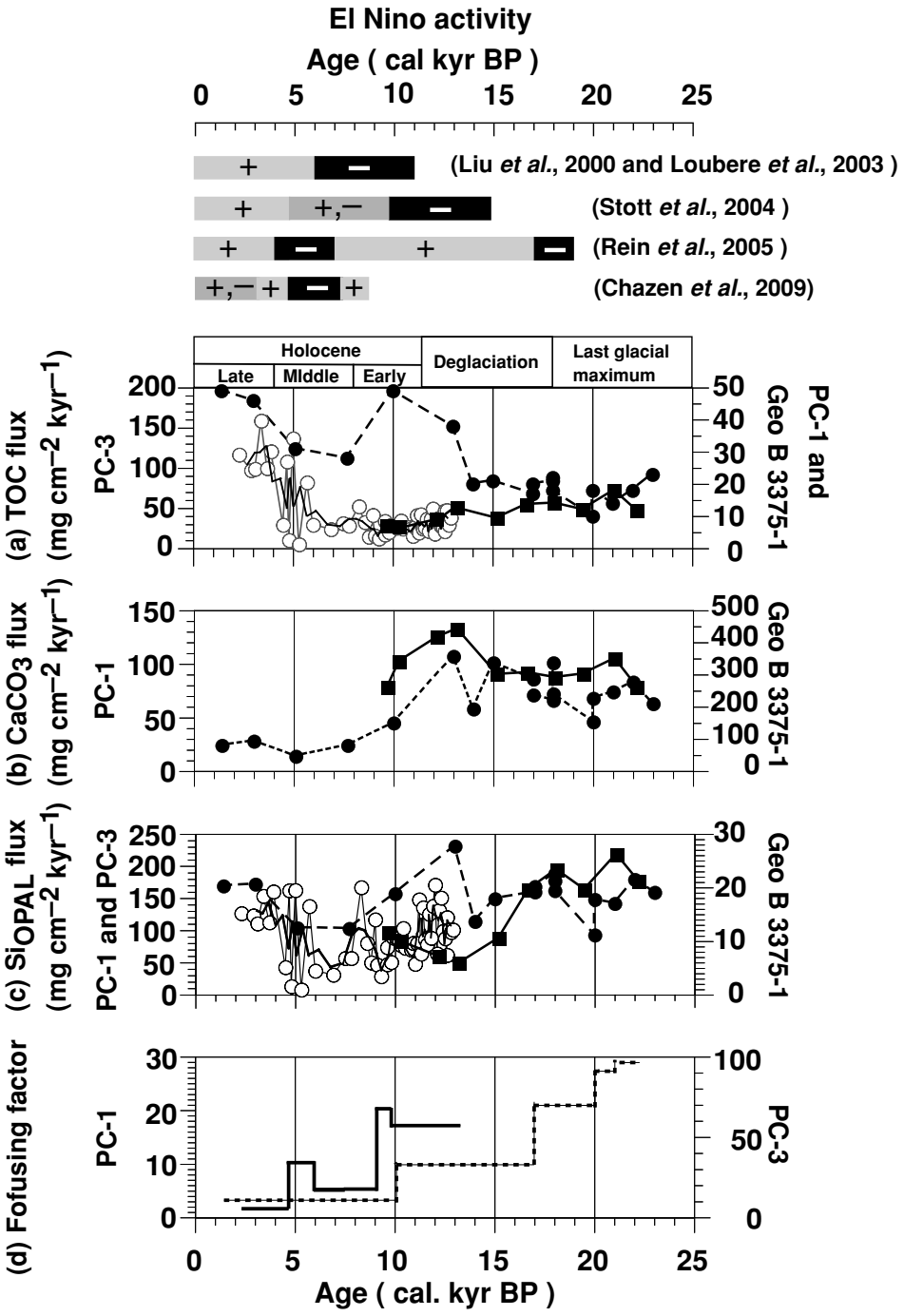

Fig. 4. ^{230}*Th-normalized fluxes of (a) TOC, (b)* $CaCO_3$*, and (c)* Si_{OPAL} *at site PC-1 (filled circles), site PC-3 (open circles), and in core GeoB3375-1 (filled squares; data from Dezileau et al., 2004). The solid lines in (a) and (c) represent three-point running averages of the PC-3 TOC and* Si_{OPAL} *flux data, respectively. (d) Changes in the focusing factor at site PC-1 (dashed line) and site PC-3 (solid line). For comparison, El Niño activity as determined by previous studies is shown at the top of the figure. A plus sign indicates predominantly El Niño-like conditions, and a minus sign indicates predominantly La Niña-like conditions.*

fective during 22–14 cal kyr BP off central Chile and during 13–6 cal kyr BP off southernmost Patagonia (Fig. 4).

SWW—a potential controlling factor of productivity

The PC-1 and PC-3 sites are located close to the northern edge and within the core of the SWW belt, respectively, which strongly affects the wind stress and precipitation along the Chilean coast. Marine and terrestrial records from oceanic and continental Chile (e.g., Heusser, 1990; Lamy *et al*., 2000; Mohtadi and Hebbeln, 2004) suggest that the moisture-bearing SWW shifted equatorward ~5° of latitude during the glacial period. Higher productivity during the LGM at 33°–35°S has been attributed previously to the equatorward migration of the SWW and a concomitant northward shift of the climate zones, resulting in equatorward displacement of the ACC, which is enriched in major nutrients (Hebbeln *et al*., 2000, 2002; Romero *et al*., 2006). Moreover, the northward shift of the SWW during the LGM would have enhanced precipitation at 27°S and 33°S, increasing the discharge of rivers, which would have transported substantial amounts of iron-rich terrigenous materials from the continent to the ocean, thus promoting high biological productivity in that region (Dezileau *et al*., 2004; Mohtadi and Hebbeln, 2004). The northward shift of the SWW during the LGM, in contrast, led to heavy increases in precipitation in the area off Concepción (36°S), thus suppressing upwelling and strengthening stratification. Low productivity during the LGM in the area off Concepción (36°S) has been attributed to nutrient deficiency due to the suppression of upwelling; an active upwelling system promoting high productivity did not develop at this latitude until the late deglaciation, after the sea-level highstand associated with Meltwater Pulse 1a was reached and the SWW had migrated back southward (Mohtadi *et al*., 2008). The ^{230}Th-normalized TOC fluxes during the LGM and the early deglaciation at the PC-1 site are thus consistent with the results reported by Mohtadi *et al*. (2008).

Modeling studies of the SWW during the LGM, on the other hand, suggest a general decrease in surface wind speeds in the Southern Ocean and sub-Antarctic sectors, rather than a real shift in the westerly circulation (Rojas *et al*., 2009). The models analyzed by Rojas *et al*. (2009) also show changes in precipitation patterns indicating a general decrease south of 40°S during the LGM. These regional heterogeneities (drier south of 40°S, but wetter in NW Patagonia) imply a zonally asymmetric Southern Hemisphere. The postglacial evolution of the SWW belt was addressed by Lamy *et al*. (2010). Based on a comparison of records from southernmost Chile in the present SWW core zone (50°–55°S) with records from the northern margin of the SWW in central Chile, their results revealed a distinct latitudinal anti-phasing of wind changes on multi-millennial time-scales: reduced early Holocene SWW at their northern margin and enhanced SWW at the core, whereas the opposite pattern is observed in the late Holocene.

From 13 to *ca*. 8 cal kyr BP at the PC-3 site, the C/N ratio was higher (~21; Fig. 3) than in the late Holocene, and Harada *et al*. (2013) reported relatively light (from –24‰ at 12 cal kyr BP to –22‰ at 8 cal kyr BP) $\delta^{13}C_{TOC}$ values during the same period, suggesting that C3 land plants ($\delta^{13}C_{C3\ plants}$, –29‰ to –25‰; Libes, 1992) contributed significantly to the TOC content. Furthermore, the LSRs (60–180 cm kyr^{-1}, Fig. 2b) and focusing factors (>50) were much higher during 13–9 cal kyr BP than later in the record. These results suggest that enhanced precipitation (associated with intensified SWW) strengthened ocean stratification during the late deglaciation and the early Holocene, reducing the effectiveness of the biological pump (low ^{230}Th-normalized fluxes of TOC) and leading to a relatively higher contribution of terrestrial compounds. In contrast, and as stated above, ^{230}Th-normalized fluxes of TOC at the PC-1 site off central Chile were low during the LGM and high during 14–8 cal kyr BP. For these periods, therefore, the two sites exhibit opposite trends. After *ca*. 5 cal kyr BP, the ^{230}Th-normalized TOC fluxes increased at both sites simultaneously and remained high thereafter.

In summary, our results point to (i) suppressed upwelling leading to strengthened ocean stratification and low productivity off central Chile (PC-1) due to intensified onshore SWW and associated increased precipitation during 22–14 cal kyr BP (as suggested by Mohtadi *et al*., 2008); (ii) high productivity off central Chile during 13 to *ca*. 8 cal kyr BP due to a more southerly position of the SWW core (conditions similar to those of the modern austral summer; Lamy *et al*., 2010) and the onset of an active upwelling system (Mohtadi *et al*., 2008); (iii) wetter conditions over southernmost Chile associated with intensified SWW (Lamy *et al*., 2010) leading to water column stratification and thus reducing productivity in southernmost Chile (PC-3 site) during 13–6 cal kyr BP; and (iv) a simultaneous increase in fluxes after *ca*. 5 cal kyr BP at the two sites, implying that the strength and position of the SWW had settled within the modern seasonal range and that the ACC supplied substantial amounts of nutrients to the ocean off central and southern Chile.

ENSO—another potential controlling factor of productivity

At present, El Niño events reduce primary productivity in the upwelling area off Chile because warmer oligotrophic waters intrude near the coast, and heavy rain and enhanced river runoff (Lima *et al*., 1999) prevent the upwelling of cold, nutrient-rich waters (Iriarte *et al*., 2000; Iriarte and González, 2004). Previous studies of El Niño

activity reconstructed from data for temperature and nutrients in the mixed layer and thermocline and from records of episodes of flooding in the eastern equatorial Pacific (EEP)–Peru upwelling region (Liu *et al*., 2000; Loubere *et al*., 2003; Rein *et al*., 2005; Chazen *et al*., 2009) and the western equatorial Pacific (Stott *et al*., 2004) generally reported (i) strong La Niña conditions during the LGM and the early and middle Holocene, and (ii) strong El Niño conditions through the deglaciation and late Holocene (~5.0 cal kyr BP) (Fig. 4). We compared the changes in the ^{230}Th-normalized biogenic components over the past 22 kyr with the findings of previous studies of El Niño activity and did not find any obvious link between variations in El Niño activity and biogenic component fluxes at the PC-1 site. In the northern Chile upwelling area, the supply of iron is an important factor controlling primary productivity (Torres and Ampuero, 2009), but the vertical variation in iron fluxes over the past 100 kyr is not in phase with Niño 3 ENSO model predictions (Dezileau *et al*., 2004). This result implies that the glacial to interglacial changes of primary productivity are not consistent with changes in ENSO intensity off Chile. ENSO affects thermocline conditions in the EEP (e.g., Makou *et al*., 2010); El Niño and La Niña promote warmer and colder thermoclines, respectively, in the EEP, and a warmer equatorial thermocline produces a deeper mixed layer, which reduces the efficiency of equatorial upwelling of cold water. This in turn weakens the coupling between the tropical ocean and the atmosphere and reduces the amplitude of ENSO (Liu *et al*., 2000). Thus, ENSO phases might be diminished if the mean equatorial thermocline is modified by the enhancement of other effects, such as seasonal forcing due to increased summer insolation either in the Northern Hemisphere generally (Liu *et al*., 2000) or locally (Loubere *et al*., 2003).

Conclusions

We investigated changes in paleoproductivity by examining ^{230}Th-normalized fluxes of the biogenic components TOC, TN, $CaCO_3$, and Si_{OPAL} in sediment cores PC-1 (covering the past 22 kyr) and PC-3 (covering the past 13 kyr) collected off the coast of central Chile and near the Pacific entrance of the Strait of Magellan, respectively. We summarize our results and possible climate mechanisms explaining them as follows:

(1) ^{230}Th-normalized fluxes of TOC at the PC-1 site were relatively low during the LGM and until ~14 cal kyr BP. A substantial increase in TOC fluxes occurred at ~13 cal kyr BP, and fluxes remained relatively high through the late Holocene except for a drop in the middle Holocene (from 8 to 5 cal kyr BP). Thus, we agree with Mohtadi *et al*. (2008) statement of the development of an active upwelling system promoting high productivity starting in the late deglaciation. At the PC-3 site, the ^{230}Th-normalized fluxes of TOC were relatively low from 13 to 6 cal kyr BP and increased thereafter. It seems likely that nutrients transported to the site by Pacific waters and a weakening of freshwater supply promoted enhancement of productivity after 6 cal kyr BP.

(2) The temporal-spatial changes in the paleo-export fluxes of biogenic components at 27°S, 36°S and 52°S off the Chilean coast imply that the biological pump was (i) effective during the LGM off northern Chile, during 15–8 cal kyr BP off central Chile, and after 5 cal kyr BP off central and southernmost Chile; and (ii) not fully effective during 22–15 cal kyr BP off central Chile and during 13–6 cal kyr BP off southernmost Patagonia.

(3) Glacial to interglacial changes of ^{230}Th-normalized biogenic components were controlled by the upwelling intensity at the PC-1 site and by the amount of nutrients supplied by Pacific water inflow at the PC-3 site. Fluxes were relatively high at the PC-1 site but low at the PC-3 site from 13 to 6 cal kyr BP. After 5 cal kyr BP, fluxes increased at both sites simultaneously. The temporal changes in biogenic component fluxes at the two sites are likely attributable to changes in the latitudinal displacement and/or changes in the intensity of the SWW during 13–6 cal kyr BP.

(4) ENSO variability apparently contributed much less to these millennial changes in productivity than SWW variability.

Acknowledgments—We are grateful to Captain Akamine, all crew members of R/V *Mirai*, and the marine technicians of Global Ocean Development Inc. and Marine Works Japan Ltd. for their proficiency in the coring operation and sample preparation during cruise MR03-K04. This paper benefited from important comments by two anonymous reviewers. This work was supported by the Japan Agency for Marine-Earth Science and Technology and, in part, by the COPAS Center of the University of Concepción. Additional financial support was provided by a Sasagawa Scientific Research Grant from the Japan Science Society.

References

Ahumada, R., Rudolph, A. and Martinez, V. (1983) Circulation and fertility of waters in Concepcion Bay. *Estuar. Coast. Shelf Sci*. **16**, 95–105.

Anderson, R. F. (1982) Concentration, vertical flux, and remineralization of particulate uranium in seawater. *Geochim. Cosmochim. Acta* **46**, 1293–1299.

Anderson, R. F. and Fleer, A. P. (1982) Determination of natural actinides and plutonium in marine particulate material. *Anal. Chem*. **54**, 1142–1147.

Anderson, R. F., Ali, S., Bradtmiller, L. I., Nielsen, S. H. H., Fleisher, M. Q., Anderson, B. E. and Burckle, L. H. (2009) Wind-driven upwelling in the Southern Ocean and the

deglacial rise in atmospheric CO_2. *Science* **323**, 1443–1448, doi:10.1126/science.1167441.

Antezana, T. (1999) Hydrographic features of Magellan and Fuegian inland passages and adjacent Subantarctic waters. *Sci. Mar.* **63**, 23–34.

Aracena, C., Carina, B. L., Jose, L. I., Lorena, R. and Silvio, P. (2011) Latitudinal patterns of export production recorded in surface sediments of the Chilean Patagonian fjords (41–55°S) as a response to water column productivity. *Cont. Shelf Res.* **31**, 340–355.

Bacon, M. P. (1984) Glacial to interglacial changes in carbonate and clay sedimentation in the Atlantic Ocean estimated from ^{230}Th measurements. *Isot. Geosci.* **2**, 97–111.

Bacon, M. P. and Anderson, R. F. (1982) Distribution of thorium isotopes between dissolved and particulate forms in the deep sea. *J. Geophys. Res.* **87**, 2045–2056.

Bacon, M. P. and Rosholt, J. N. (1982) Accumulation rates of Th-230, Pa-231 and some transition metals on the Bermuda Rise. *Geochim. Cosmochim. Acta* **46**, 651–666.

Broecker, W. S. (1982) Ocean chemistry during glacial time. *Geochim. Cosmochim. Acta* **46**, 1689–1705.

Chaigneau, A. and Pizarro, O. (2005) Surface circulation and fronts of the South Pacific Ocean, east of 120 degrees W. *Geophys. Res. Lett.* **32**(8), L08605, doi:10.1029/2004GL022070.

Chase, Z., Anderson, R. F., Fleisher, M. Q. and Kubik, P. W. (2003) Scavenging of ^{230}Th, ^{231}Pa and ^{10}Be in the Southern Ocean (SW Pacific sector): the importance of particle flux, particle composition and advection. *Deep-Sea Res. II* **50**, 739–768.

Chazen, C. R., Altabet, M. A. and Herbert, T. D. (2009) Abrupt mid-Holocene onset of centennial-scale climate variability on the Peru–Chile Margin. *Geophys. Res. Lett.* **36**, L18704, doi:10.1029/2009GL039749.

Chen, J. H., Lawrence Edwards, R. and Wasserburg, G. J. (1986) ^{238}U, ^{234}U and ^{232}Th in seawater. *Earth Planet. Sci. Lett.* **80**, 241–251.

Clark, P. U., Dyke, A. S., Shakun, J. D., Carlson, A. E., Clark, J., Wohlfarth, B., Mitrovica, J. X., Hostetler, S. W. and McCabe, A. M. (2009) The last glacial maximum. *Science* **325**, 410–714.

Conkright, M. E., Levitus, S. and Boyer, T. P. (1994) World Ocean Atlas, Volume 1: nutrients. NOAA Atlas NESDIS, Vol. 1. U.S. Department of Commerce, Washington, D.C., U.S.A., 150 pp.

Daneri, G., Dellarossa, V., Quiñones, R., Jacob, B., Montero, P. and Ulloa, O. (2000) Primary production and community respiration in the Humboldt Current System off Chile and associated oceanic areas. *Mar. Ecol. Prog. Ser.* **197**, 41–49.

Dezileau, L., Ulloa, O., Hebbeln, D., Lamy, F., Reyss, J. and Fontugne, M. (2004) Iron control of past productivity in the coastal upwelling system off the Atacama Desert, Chile. *Paleoceanography* **19**, PA3012, doi:10.1029/2004PA001006.

Fernández, C., Farías, L. and Alcaman, M. E. (2009) Primary production and nitrogen regeneration processes in surface waters of the Peruvian upwelling system. *Prog. Oceanogr.* **83**, 159–168.

François, R. (2007) Paleoflux and paleocirculation from sediment ^{230}Th, and ^{231}Pa/^{230}Th. *Development in Marine Geology* (Hillaire-Marcel, C. and De Vernal, A., eds.), **1**, doi:10.1016/S1572-5480(07)01021-4.

François, R., Altabet, M. A., Yu, E.-F., Sigman, D. M., Bacon, M. P., Frank, M., Bohrmann, G., Bareille, G. and Labeyrie, L. D. (1997) Contribution of Southern Ocean surface-water stratification to low atmospheric CO_2 concentrations during the last glacial period. *Nature* **289**, 929–935, doi:10.1038/40073.

François, R., Frank, M. and Rutgers van der Loeff, M. M. (2004) ^{230}Th normalization: An essential tool for interpreting sedimentary fluxes during the late Quaternary. *Paleoceanography* **19**, PA1018, doi:10.1029/2003PA000939.

Harada, N., Ahagon, N., Lange, C. B., Asahara, Y., Pantoja, S., Marchant, M. E., Mishima, T., Kanke, H., Tapia, R. I., Sepulueda, J., Santis, A. J. A., Katsuki, K., Matsuura, Y., Sato, Y., Maeda, R., Ueno, T., Tokunaga, W., Kimura, R. and Nagahama, N. (2005) Basic physical properties of sediment cores collected in the Chilean marginal area and Magellan Strait during leg. 3 of cruise MR03-K04. *JAMSTEC Report of Research and Development* **2**, 13–27.

Harada, N., Kawakami, H., Fukuda, M., Miyashita, W. and Matsumoto, T. (2012) ^{230}Th-normalized fluxes of biogenic components from the central Chilean Margin during the Late Quaternary. *Journal of Geography* (*Chigaku Zasshi*), **121**(3), 555–569 (in Japanese with English abstract).

Harada, N., Ninnemann, U., Lange, C. B., Marchant, M. E., Sato, M., Ahagon, N. and Pantoja, S. (2013) Deglacial–Holocene environmental changes at the Pacific entrance of the Strait of Magellan. *Palaeogeogr. Palaeoclimatol. Palaeoecol.*, doi:10.1016/j.palaeo.2013.02.022 (in press).

Hebbeln, D., Marchant, M., Freudenthal, T. and Wefer, G. (2000) Surface sediment distribution along the Chilean continental slope related to upwelling and productivity. *Mar. Geol.* **164**, 119–137.

Hebbeln, D., Marchant, M. and Wefer, G. (2002) Paleoproductivity in the southern Peru–Chile Current through the last 33,000 yr. *Mar. Geol.* **186**, 487–504.

Henderson, G. M. and Anderson, R. F. (2003) The U-series toolbox for paleoceanography. *Rev. Min. Geochem.* **52**, 493–531.

Henderson, G. M., Heinze, C., Anderson, R. F. and Winguth, A. M. E. (1999) Global distribution of the ^{230}Th flux to ocean sediments constrained by GCM modeling. *Deep-Sea Res. I* **46**, 1861–1893.

Heusser, C. J. (1990) Ice age vegetation and climate of subtropical Chile. *Palaeogeogr. Palaeoclimatol. Palaeoecol.* **80**, 107–127.

Ingram, B. L. and Southon, J. R. (1996) Reservoir ages in Eastern Pacific coastal and estuarine waters. *Radiocarbon* **38**, 573–582.

Iriarte, J. L. and González, H. E. (2004) Phytoplankton size structure during and after the 1997/98 El Niño in a coastal upwelling area of the northern Humboldt Current System. *Mar. Ecol. Prog. Ser.* **269**, 83–90.

Iriarte, J. L., Pizarro, G., Troncoso, V. A. and Sobarzo, M. (2000) Primary production and biomass of size-fractionated phytoplankton off Antofagasta, Chile (23–24°S) during pre-

El Niño and El Niño 1997. *J. Mar. Syst.* **26**, 37–51.
Iriarte, J. L., Vargas, C. A., Tapia, F. J., Bermúdez, R. and Urrutia, R. E. (2007) Primary production and plankton carbon biomass in a river-influenced upwelling area off Concepción, Chile. *Prog. Oceanogr.* **92–95**, 97–109.
Kawakami, H. and Honda, M. C. (2007) Time-series observation of POC fluxes estimated from ^{234}Th in the northwestern North Pacific. *Deep-Sea Res. I* **54**, 1070–1090.
Kilian, R., Baeza, O., Steinke, T., Arevalo, M., Rios, C. and Schneider, C. (2007) Late Pleistocene to Holocene marine transgression and thermohaline control on sediment transport in the western Magellanes fjord system of Chile (53°S). *Quat. Internat.* **161**, 90–107.
Kohfeld, K. E., Le Quéré, C., Harrison, S. P. and Anderson, R. F. (2005) Role of marine biology in glacial–interglacial CO_2 cycles. *Science* **308**, 74–78.
Lambeck, K., Yokoyama, Y. and Purcell, T. (2002) Into and out of the Last Glacial Maximum: sea-level change during Oxygen Isotope Stages 3 and 2. *Quat. Sci. Rev.* **21**, 343–360.
Lamy, F., Hebbeln, D. and Wefer, G. (1999) High resolution marine record of climatic change in mid-latitude Chile during the last 28,000 years based on terrigenous sediment parameters. *Quat. Res.* **51**, 83–93.
Lamy, F., Hebbeln, D., Wefer, G. and Marchant, M. (2000) Reconstructing latitudinal shifts of the Southern Westerlies from marine sediment studies along the Chilean continental margin. *PAGES Newsletter* **2000-2**, 8–9.
Lamy, F., Kilian, R., Arz, H. W., Francois, J.-P., Kaiser, J., Prange, M. and Steinke, T. (2010) Holocene changes in the position and intensity of the Southern Westerly wind belt. *Nature Geoscience* **3**, 695–699, doi:10.1038/NGEO959.
Libes, S. M. (1992) *An Introduction to Marine Biogeochemistry*. John Wiley & Sons, Inc., New York, 734 pp.
Lima, M., Marquet, P. A. and Jaksic, F. M. (1999) El Niño events, precipitation patterns, and rodent outbreaks are statistically associated in semiarid Chile. *Ecography* **22**, 213–218.
Liu, Z., Kutzbach, J. and Wu, L. (2000) Modeling climate shift of El Niño variability in the Holocene. *Geophys. Res. Lett.* **27**, 2265–2268.
Loubere, P., Mathieu, R., Liu, Z. and Mekik, F. (2003) Oceanic conditions in the eastern equatorial Pacific during the onset of ENSO in the Holocene. *Quat. Res.* **60**, 142–148.
Loubere, P., Mekik, F., François, R. and Pichat, S. (2004) Export fluxes of calcite in the eastern equatorial Pacific from the Last Glacial Maximum to present. *Paleoceanography* **19**, PA2018, doi:10.1029/2003PA000986.
Lyle, M., Mitchell, N., Pisias, N., Mix, A., Martinez, J. I. and Paytan, N. (2005) Do geochemical estimates of sediment focusing pass the sediment test in the equatorial Pacific? *Paleoceanography* **20**, PA1005, doi:10.1029/2004PA001019.
Lyle, M., Pisias, N., Paytan, A., Martinez, J. I. and Mix, A. (2007) Reply to comment by R. Francois *et al.* on "Do geochemical estimates of sediment focusing pass the sediment test in the equatorial Pacific?": Further explorations of ^{230}Th normalization. *Paleoceanography* **22**, PA1217, doi:10.1029/2006PA001373.
Magazzù, G., Panella, S. and Decembrini, F. (1996) Seasonal variability of fractionated phytoplankton, biomass and primary production in the Straits of Magellan. *J. Mar. Syst.* **9**, 249–267.
Makou, M. C., Eglinton, T. I., Oppo, D. W. and Hughen, K. A. (2010) Postglacial changes in El Niño and La Niña behavior. *Geology* **38**, 43–46.
Marchant, M., Hebbeln, D. and Wefer, G. (1999) High resolution planktic foraminiferal record of the last 13,300 years from the upwelling area off Chile. *Mar. Geol.* **161**, 115–128.
Martin, J. (1990) Glacial–interglacial CO_2 change: The iron hypothesis. *Paleoceanography* **5**, 1–13.
Mayewski, P. A., Rohling, E. E., Stager, J. C., Karlén, W., Maasch, K. A., Meeker, L. D., Meyerson, E. A., Gasse, F., van Kreveld, S., Holmgren, K., Lee-Thorp, J., Rosqvist, G., Rack, F., Staubwasser, M., Schneider, R. R. and Steig, E. J. (2004) Holocene climate variability. *Quat. Res.* **62**, 243–255.
McElroy, M. B. (1983) Marine biological controls on atmospheric CO_2 and climate. *Nature* **302**, 328–329.
Messié, M., Ledesma, J., Kolber, D. D., Michisaki, R. P. and Chavez, F. P. (2009) Potential new production in four eastern boundary upwelling systems. *Prog. Oceanogr.* **83**, 151–158.
Meyers, P. A. (1994) Preservation of elemental and isotopic source identification of sedimentary organic matter. *Chem. Geol.* **114**, 289–302.
Mohtadi, M. and Hebbeln, D. (2004) Mechanisms and variations of the paleoproductivity off northern Chile (24°S–33°S) during the last 40,000 years. *Paleoceanography* **19**, PA2023, doi:10.1029/2004PA001003.
Mohtadi, M., Rossel, P., Lange, C. B., Pantoja, S., Boning, P., Repeta, D. J., Grunwald, M., Lamy, F., Hebbeln, D. and Brumsack, H. (2008) Deglacial pattern of circulation and marine productivity in the upwelling region off central-south Chile. *Earth Planet. Sci. Lett.* **272**, 221–230.
Montecino, V., Astoreca, R., Alarcón, G., Rentamal, L. and Pizarro, G. (2004) Bio-optical characteristics and primary productivity during upwelling and non-upwelling conditions in a highly productive coastal ecosystem off central Chile (~36°S). *Deep-Sea Res. II* **51**, 2413–2426.
Montero, P., Daneri, G., Cuevas, L. A., González, H. E., Jacob, B., Lizárraga, L. and Menschel, E. (2007) Productivity cycles in the coastal upwelling area off Concepción: the importance of diatoms and bacterioplankton in the organic carbon flux. *Prog. Oceanogr.* **75**(3), doi:10.1016/j.pocean.2007.08.013.
Mortlock, R. A. and Froelich, P. N. (1989) A simple method for the rapid determination of biogenic opal in pelagic marine sediments. *Deep-Sea Res. I* **36**, 1415–1426.
Müller, P. J. and Schneider, R. (1993) An automated leaching method for the determination of opal in sediments and particulate matter. *Deep-Sea Res. I*, **40**, 425–444.
Muratli, J. M., Chase, Z., Mix, A. C. and McManus, J. (2010) Increased glacial-age ventilation of the Chilean margin by Antarctic Intermediate Water. *Nature Geoscience* **3**, doi:10.1038/NGEO715.
Narita, H., Abe, R., Tate, K., Kim, Y. I., Harada, K. and Tsunogai, S. (2003) Anomalous large scavenging of ^{230}Th

and ^{231}Pa controlled by particle composition in the northwestern North Pacific. *J. Oceanogr.* **59**, 739–750.

Orsi, A. H., Whitworth, T. and Nowlin, W. D. (1995) On the meridional extent and fronts of the Antarctic Circumpolar Current, *Deep-Sea Res. I* **42**, 641–673.

Oyarzrum, S., Marin, S., Valladares, C. and Iriarte, J. L. (1999) Reproductive cycle of *Loxechimus albus* (Echinodermata: Echinoidea) in two areas of the Magellan Region (53°S, 70°–72°W), Chile. *Sci. Mar.* **63**, 439–449.

Pickard, G. L. (1971) Some physical oceanographic features of inlets of Chile. *J. Fish. Res. Board Can.* **28**, 1077–1106.

Pineda, V. (1999) El cañón submarino del Río Bio-Bio: Aspectos dinámicos y ambientales. Ph.D. Thesis, Centro EULA, Universidad de Concepción, Chile.

Rein, B., Lückge, A., Reinhardt, L., Sirocko, F., Wolf, A. and Dullo, W. (2005) El Niño variability off Peru during the last 20,000 years. *Paleoceanography* **20**, PA4003, doi:10.1029/2004PA001099.

Robinson, R. S., Sigman, D. M., DiFiore, P. J., Rohde, M. M., Mashiotta, T. A. and Lea, D. W. (2005) Diatom-bound ^{15}N/^{14}N: New support for enhanced nutrient consumption in the ice age subantarctic. *Paleoceanography* **20**, PA3003, doi:10.1029/2004PA001114.

Rojas, M., Moreno, P., Kageyama, M., Crucifix, M., Hewitt, C., Abe-Ouchi, A., Ohgaito, R., Brady, E. C. and Hope, P. (2009) The Southern Westerlies during the last glacial maximum in PMIP2 simulations. *Clim. Dyn.* **32**, 525–548, doi:10.1007/s00382-008-0421-7.

Romero, O. E., Kim, J.-H. and Hebbeln, D. (2006) Paleoproductivity evolution off central Chile from the Last Glacial Maximum to the Early Holocene. *Quat. Res.* **65**, 519–525.

Shaffer, G., Salinas, S., Pizarro, O., Vega, A. and Hormazabal, S. (1995) Currents in the deep ocean off Chile (30°S). *Deep-Sea Res.* **42**, 425–436, doi:10.1016/0967-0637(95)99823-6.

Sievers, H. A. and Silva, N. (2008) Water masses and circulation in austral Chilean channels and fjords. *Progress in the Oceanographic Knowledge of Chilean Interior Waters, from Puerto Montt to Cape Horn* (Silva, N. and Palma, S., eds.), 53–58, Comité Oceanográfico Nacional-Pontificia Universidad Católica de Valparaíso.

Sigman, D. M., Hain, M. P. and Haug, G. H. (2010) The polar ocean and glacial cycles in atmospheric CO_2 concentration. *Nature* **466**, 47–55, doi:10.1038/nature09149.

Silva, N. and Calvete, C. (2002) Physical and chemical oceanographic features of southern Chilean inlets between Penas Gulf and Magellan Strait (CIMAR-FIORDO 2 CRUISE). *Ciencia y Tecnología del Mar* **25**, 23–28.

Sobarzo, M., Bravo, L., Donoso, D., Garcés-Vargas, J. and Schneider, W. (2007) Coastal upwelling and seasonal cycles that influence the water column over the continental shelf off central Chile. *Prog. Oceanogr.* **75**, 363–383.

Stott, L., Cannariato, K., Thunell, R., Haug, G. H., Koutavas, A. and Lund, S. (2004) Decline of surface temperature and salinity in the western tropical Pacific Ocean in the Holocene epoch. *Nature* **431**, 56–59.

Strub, P. T., Mesías, J. M., Montecino, V., Rutllant, J. and Salinas, S. (1998) Coastal ocean circulation off western South America. *The Global Coastal Ocean-Regional Studies and Synthesis. The Sea, Ideas and Observations on Progress in the Study of the Seas* (Robinson, A. R. and Brink, K. H., eds.), 273–313, John Wiley & Sons, Inc., New York.

Stuiver, M. and Polach, H. A. (1977) Reporting of 14-C data. *Radiocarbon* **19**, 355–363.

Suman, D. O. and Bacon, M. P. (1989) Variations in Holocene sedimentation in the North American basin determined from ^{230}Th measurements, *Deep-Sea Res.* **36**, 869–878.

Torres, R. and Ampuero, P. (2009) Strong CO_2 outgassing from high nutrient low chlorophyll coastal waters off central Chile (30°S): The role of dissolved iron. *Estuar. Coast. Shelf Sci.* **83**, 126–132.

Weninger, B., Jöris, O. and Danzeglocke, U. (2009) CalPal-2007. Cologne Radiocarbon Calibration & Palaeoclimate Research Package. Available at http://www.calpal.de/ (accessed 2009-01-10).

Yokoyama, Y. and Esat, T. M. (2011) Global climate and sea level: Enduring variability and rapid fluctuations over the past 150,000 years. *Oceanography* **24**, 54–69.

Yu, E.-F., Francois, R., Bacon, M. P. and Fleer, A. P. (2001) Fluxes of ^{230}Th and ^{231}Pa to the deep sea: Implications for the interpretation of excess ^{230}Th and ^{231}Pa/^{230}Th profiles in sediments. *Earth Planet. Sci. Lett.* **191**, 219–230.

Supplementary Materials

URL (http://www.terrapub.co.jp/journals/GJ/archives/data/47/MS230.pdf)
Tables S1 to S2